Comparative analysis of radiative transfer approaches for calculation of diffuse reflectance of plane-parallel light-scattering layers

Leonid G. Sokoletsky,[1,2,*] Alexander A. Kokhanovsky,[3,4] and Fang Shen[5]

[1]SPE "LAZMA" Ltd., Tvardovsky Street 8, Technopark "Strogino," Moscow 125252, Russian Federation; currently at

[2]State Key Laboratory of Estuarine and Coastal Research, East China Normal University, Shanghai 200062, China

[3]Institute of Remote Sensing, University of Bremen, O. Hahn Allee 1, D-28334 Bremen, Germany; currently at

[4]EUMETSAT, Eumetsat Allee 1, D-64295 Darmstadt, Germany

[5]State Key Laboratory of Estuarine and Coastal Research, East China Normal University, Shanghai 200062, China

*Corresponding author: sokoletsky.leonid@gmail.com

Received 3 June 2013; revised 27 September 2013; accepted 8 October 2013;
posted 28 October 2013 (Doc. ID 191006); published 4 December 2013

We present an analysis of a number of different approximations for the diffuse reflectance (spherical and plane albedo) of a semi-infinite, unbounded, plane-parallel, and optically homogeneous layer. The maximally wide optical conditions (from full absorption to full scattering and from fully forward to fully backward scattering) at collimated, diffuse, and combined illumination conditions were considered. The approximations were analyzed from the point of view of their physical limitations and compared to the numerical radiative transfer solutions, whenever it was possible. The main factors impacting the spherical and plane albedo were revealed for the known and unknown scattering phase functions. The main criterion for inclusion of the models in analysis was the possibility of practical use, i.e., approximations were well parameterized and only included easily measured or estimated parameters. We give a detailed analysis of errors for different models. An algorithm for recalculation of results under combined (direct and diffuse) illumination also has been developed.

OCIS codes: (030.5620) Radiative transfer; (120.5700) Reflection; (290.7050) Turbid media.
http://dx.doi.org/10.1364/AO.52.008471

1. Introduction

An estimation of the reflected and transmitted light in turbid medium as a function of layer thickness, illumination, and observation conditions, along with the inherent optical properties (IOPs) of the medium, is a main step to a solution of many different problems. Examples of such problems are an estimation of the amounts of various substances dissolved and suspended in natural waters, noninvasive determination of the optical absorption and scattering properties of human tissue, evaluation of particle size distribution, and refractive indices of pigments and other particles in paint and varnish, calibration of optical instruments, etc. However, in many cases direct measurements of IOPs are difficult; for example, in cases of medical diagnostics or ocean color remote sensing. In such cases, measurements of apparent optical properties such as reflectance and transmittance remain the main sources of information about the target under investigation. Therefore the use of indirect methods and algorithms for the conversion of measured reflectance and transmittance into IOPs is still an utmost issue.

1559-128X/13/358471-13$15.00/0

Though a large number of such methods have been developed over the last century in the radiative transfer theory and such applicative fields as astrophysics, ocean and atmospheric optics, biomedical optics, chemistry-technological optics etc., the selection of simple and accurate methods remains a nontrivial task for many investigators. One of the reasons for this consists in using very different systems of approaches and nomenclatures in different scientific fields. Our purpose was to express these different approaches and nomenclatures to the common language. In the current work, we focus on an analysis of the accuracy for different optical models and their combinations, limiting ourselves to consideration of reflected light in plane-parallel homogeneous unbounded layers. Additionally, we considered only models for collimate (at incidence angles smaller than 45°) or diffuse incoming light and diffuse collected light. Such conditions are fulfilled in the most real situations, especially if we consider propagation and reflection of light in the media with the refractive indices different from this of the air. The majority of the models have been selected from numerous literature sources, while several other models have been developed for the first time.

We consider this study as a continuation of the previous studies attempting to compare different numerical and analytical radiative transfer reflectance approximations [1–13] with the aim of seeking simple but reliable solutions. We put forward a task to yield a comprehensive review of the radiative transfer approximations for diffuse reflectance, especially in their analytical form, which is convenient for fast routine calculations. This purpose responds to the utmost requirements of many various fields of knowledge.

2. Main Definitions

We will consider diffuse reflectance (plane and spherical albedo) in plane-parallel homogeneous unbounded layers illuminated by an external light source. Thus we neglect the refractive index mismatch between the plane-parallel layer and the surrounding medium. However, readers interested in how to account accurately for this mismatch are invited to use algorithms described by numerous authors beginning from Saunderson [14] and his followers [15–17]. Both types of illumination (direct and diffuse) with the diffusely collected reflected light will be considered. Finally, we show how to deal with the combined (direct and diffuse) illumination.

A. Plane Albedo

The plane albedo R_p is defined as the ratio of radiation reflected diffusively from the layer to the incoming direct radiation. This optical property is often called by other names such as "directional-hemispherical reflectance," "hemispherical albedo," "hemispherical reflectance," and "diffuse reflectance of the surface, illuminated by the direct rays." We use the term "plane albedo," which is more acceptable in publications on radiative transfer. The plane albedo for an infinite layer is defined as [9,18–20]

$$R_p(\mu_i) = \frac{1}{\pi}\int_0^{2\pi}\int_0^1 R(\mu_i,\mu_v,\varphi)\mu_v \mathrm{d}\mu_v \mathrm{d}\varphi, \tag{1}$$

where μ_i is the cosine of the incidence angle θ_i in the medium, μ_v is the cosine of the viewing angle θ_v in the medium, and φ is the azimuthal angle between the incident and scattered beam directions. The reflectance factor $R(\mu_i,\mu_v,\varphi)$ is defined [20,21] as the ratio of the intensity of light reflected from a given layer to the intensity of light reflected from the Lambertian absolutely white surface. For the practical aims, it is suitable to use an azimuthally averaged reflectance factor $\bar{R}(\mu_i,\mu_v)$ [11] as follows:

$$\begin{aligned} R_p(\mu_i) &= 2\int_0^1 \bar{R}(\mu_i,\mu_v)\mu_v \mathrm{d}\mu_v, \\ \bar{R}(\mu_i,\mu_v) &= \frac{1}{2\pi}\int_0^{2\pi} R(\mu_i,\mu_v,\varphi)\mathrm{d}\varphi. \end{aligned} \tag{2}$$

Five physical limitations may be imposed on $R_p(\mu_i)$ [22–24]: (1) $R_p(\mu_i) = 0$ at the single-scattering albedo $\omega_0 = b/(a+b) = b/c = 0$; (2) $R_p(\mu_i) = 1$ at $\omega_0 = 1$; (3) $0 < R_p(\mu_i) < 1$ for $0 < \omega_0 < 1$; (4) $\partial R_p(\mu_i,\omega_0)/\partial\omega_0 \geq 0$; and (5) $\partial R_p(\mu_i,B)/\partial B \geq 0$.

Here a, b, and c are coefficients of absorption, scattering, and attenuation, respectively. Table 1 contains these and several other IOPs used in this study. Note also that although the $R_p(\mu_i) \leq 1$, $R(\mu_i,\mu_v,\varphi)$ may be >1 at ω_0 close to 1 [23,24].

B. Spherical Albedo

The spherical albedo r is another type of reflectance at which incoming and reflected light are diffused. In the literature, other names of this physical quantity like "global albedo," "diffuse-diffuse reflectance," and "spherical reflectance" may be met. The spherical albedo for an infinite layer is defined as [9,18,20,25]

$$r = 2\int_0^1 R_p(\mu_i)\mu_i \mathrm{d}\mu_i = 4\int_0^1\int_0^1 \bar{R}(\mu_i,\mu_v)\mu_i\mu_v \mathrm{d}\mu_i \mathrm{d}\mu. \tag{3}$$

From Eq. (3) it follows that r does not depend on the angular conditions of illumination or observation; thus it may be considered as an IOP of the medium. Five physical limitations similar to this were imposed on the $R_p(\mu_i)$ and may also be applied for r: (1) $r = 0$ at the $\omega_0 = 0$; (2) $r = 1$ at $\omega_0 = 1$; (3) $0 < r < 1$ for $0 < \omega_0 < 1$; (4) $\partial r(\omega_0)/\partial\omega_0 \geq 0$; and (5) $\partial r(\mu_i,B)/\partial B \geq 0$.

3. Calculation Methods and Numerical Results

A. Scattering Phase Functions

Three different scattering phase functions $p(\theta)$ (Fig. 1) have been used in our study for modeling reflective and transmitted properties of the layer:

Table 1. Compendium of IOPs Used in the Work and Their Mathematical Definitions

Name of Optical Property	Symbol	Definition
Absorption coefficient (m^{-1})	a	
Scattering coefficient (m^{-1})	b	$b = b_f + b_b$
Attenuation coefficient (m^{-1})	c	$c = a + b$
Single-scattering albedo	ω_0	$\omega_0 = \frac{b}{c} = \frac{b}{a+b}$
Backscattering coefficient (m^{-1})	b_b	$b_b = 2\pi \int_{\pi/2}^{\pi} \beta(\theta) \sin\theta \mathrm{d}\theta$, where $\beta(\theta)$ is the volume scattering function at the light propagation angle θ
Forward scattering coefficient (m^{-1})	b_f	$b_f = 2\pi \int_{0}^{\pi/2} \beta(\theta) \sin\theta \mathrm{d}\theta$
Backscattering probability	B	$B = \frac{b_b}{b} = \frac{1}{2} \int_{\pi/2}^{\pi} p(\theta) \sin\theta \mathrm{d}\theta$, where $p(\theta)$ is the scattering phase function
Forward scattering probability	F	$F = \frac{b_f}{b} = 1 - B = \frac{1}{2} \int_{0}^{\pi/2} p(\theta) \sin\theta \mathrm{d}\theta$
Scattering asymmetry parameter	g	$g = \frac{1}{2} \int_{0}^{\pi} p(\theta) \sin\theta \cos\theta \mathrm{d}\theta$ this parameter may also be expressed through the refractive indices of particles and the medium, wavelength, and particle sizes (i.e., by Mie theory)
Transport (reduced) scattering coefficient (m^{-1})	b_{tr}	$b_{\mathrm{tr}} = b(1-g)$
Scattering phase function	$p(\theta)$	$p(\theta) = \frac{\beta(\theta)}{b}$
Gordon's parameter	G	$G = \frac{b_b}{a+b_b} = \frac{B\omega_0}{1-F\omega_0}$
Similarity (Hulst's) parameter	s	$s = \sqrt{\frac{1-\omega_0}{1-g\omega_0}} = \sqrt{1-\omega_{\mathrm{tr}}}$
Transport (reduced) single-scattering albedo	ω_{tr}	$\omega_{\mathrm{tr}} = \frac{b_{\mathrm{tr}}}{a+b_{\mathrm{tr}}} = \frac{(1-g)\omega_0}{1-g\omega_0}$
Diffuse absorption coefficient (m^{-1})	K	Defined in the frame of the two-flux Gurevich–Kubelka–Munk (GKM) theory
Diffuse scattering coefficient (m^{-1})	S	Defined in the frame of the GKM theory
Thennadil's parameter	C_0	$C_0 = 4.8446 + 0.472g - 0.114g^2$
Hapke's reflectance parameter	r_0	$r_0 = \frac{1-\sqrt{1-\omega_0}}{1+\sqrt{1-\omega_0}}$
Wu's parameter	W	$W = -\frac{\ln\omega_0}{1-g}$
Conversion absorption parameter	η	$\eta = a/K$
Chandrasekhar–Klier parameter	ξ	$\omega_{\mathrm{tr}} = \frac{2\xi}{\ln[(1+\xi)/(1-\xi)]}$
Conversion-scattering parameter	χ	$\chi = b_{\mathrm{tr}}/S$
Haltrin's parameter	Ψ	$\Psi = \left[1 + (4+2\sqrt{2})(b_b/a)\right]^{-1/2} = \left[\frac{1-G}{1+(3+2\sqrt{2})G}\right]^{1/2}$
Rozenberg's parameter	y	$y = \sqrt{\frac{1-\omega_0}{1-g}}$

We used two optical properties for characterization of $p(\theta)$; namely, scattering asymmetry parameter g and backscattering probability B as follows: (1) $g = 0.0019$, $B = 0.4986$ (the $p(\theta)$ with such parameters corresponding to the case of the balance between the forward and back scattering); (2) $g = 0.5033$, $B = 0.1559$ (process of forward scattering is prevailing); (3) $g = 0.9583$, $B = 0.0087$ (process of backscattering is almost negligible compared to forward scattering). The $p(\theta)$ have been calculated using exact Mie theory for spherical particles distributed in the medium according to the gamma particle size distribution [9,24] for different values of the effective radius r_{eff} and particles (relative to medium) of refractive indices $m = n - i\chi$ (at the wavelength of 550 nm) as specified in Table 2. Only models satisfying the above-mentioned physical limitations were included in the final tables. For comparison, we plot also Henyey–Greenstein $p(\theta)$ [26] computed for the same values of B as selected $p(\theta)$, but for g values ensuring a maximal closness to the selected $p(\theta)$.

Accuracy of the approximated models was evaluated by computing the mean absolute percentage error (MAPE) and the normalized (to the standard deviation s) root-mean-square error (NRMSE):

$$\mathrm{MAPE}(\%) = 100\% \frac{\sum_{i=1}^{n} |(\tilde{x}_i - x_i)/\tilde{x}_i|}{n}, \qquad (4)$$

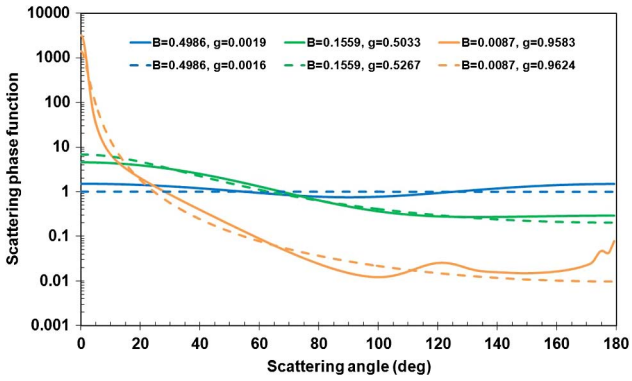

Fig. 1. Scattering phase functions $p(\theta)$ used for modeling. The main selected $p(\theta)$ is shown by solid lines, while corresponding Henyey–Greenstein $p(\theta)$ (with the same B values) is shown by dash lines.

$$\mathrm{NRMSE}(\%) = 100\% \frac{\sqrt{\sum_{i=1}^{n} \frac{(\tilde{x}_i - x_i)^2}{n-1}}}{\bar{x}}, \tag{5}$$

where $\tilde{x}_i$ and x_i are the analytical (approximated) and numerical (accepted as a reference) values of the optical property under investigation, respectively; $\bar{x}$ is the averaged value for all x_i values derived for a given phase function $p(\theta)$. The MAPE yields an averaged absolute error, while the NRMSE indicates whether the prediction is better than a simple mean prediction. An NRMSE = 0 indicates predictions are perfect, and an NRMSE = 1 indicates that the prediction is no more accurate than taking the mean of numerical results for given modeling parameters.

B. Plane Albedo Modeling

Seven various approximations for R_p derived by a number of authors and three approximations derived currently for the first time were examined for their accuracy (Table 3, Figs. 2–5). We used for computations three different $p(\theta)$ described above. The values of ω_0 for modeling were taken from the range of 0.1,0.2…0.9, 0.95, 0.99, 0.999, 0.9999, while values of μ_i were taken almost evenly (51 values) within the range from 0.70 to 1. However, in a final analysis we used only three different ranges for the ω_0; namely, $0.1 \le \omega_0 \le 0.6$, $0.6 \le \omega_0 \le 0.9$, and $0.9 \le \omega_0 \le 1$, and only one value of $\mu_i = \cos 30.5° = 0.862$. A reason for the last choice is a rather flat dependence $R_p(\mu_i)$, excluding the range of $\theta_i > 180° - \theta_r$ where θ_r is the rainbow scattering angle. The reasonable range for the θ_r values [27–29] is from 114° to 124° at the selected values of refractive indices n (Table 2). Therefore, $\theta_i = 30.5°$ is approximately the middle of the zone free from the rainbow effect. This θ_i value corresponds to 42.8° for the angle of incidence from the air to water (with refractive index $n = 1.34$) and 49.6° for the incidence angle from the air to glass ($n = 1.5$), which are typical values for many optical applications. Such choice of parameters allows obtaining some conclusions for the very different scattering media.

Table 2. Parameters Used for the $p(\theta)$ Generation

g	B	r_{eff} (μm)	n	χ
0.0019	0.4986	0.006	1.2	0
0.5033	0.1559	0.116	1.25	0.001
0.9583	0.0087	5	1.2	0.01

All plane albedo approximation models have been compared with the results derived by using the invariant imbedding method (IIM) described in detail by Mishchenko *et al.* (1999) [30] and Sokoletsky *et al.* (2009) [12]. This method has been verified previously [12] for two very distinct scattering phase functions (the Rayleigh and Fournier–Forand–Mobley phase functions with $g = 0.00$ and $g = 0.94$, respectively) by comparison of the plane albedo IIM computations with two other numerical methods (namely, different variants of the discrete ordinate method). Divergence of the results was within 1.8% for any combination of geometrical and optical parameters.

Below we give a derivation of new approximations used for the plane albedo modeling.

1. *Replacement Method*

An idea of this method is a replacement of computation for the plane albedo $R_p(\mu_i)$ by the computation for the spherical albedo r. Taking into account that dependences of $R_p(\mu_i)$ are strictly monotonic, and the "effective" angles $\theta_{i,\mathrm{ef}} = \arccos \mu_{\mathrm{ef}}$ at which $R_p(\mu_{\mathrm{ef}}) = r$ lie generally in the range from 48° to 61° [10], a procedure of $R_p(\mu_i)$ calculation may be presented as

$$R_p(\mu_i) = r \frac{R_p(\mu_i)/R_p(1)}{R_p(\mu_{\mathrm{ef}})/R_p(1)}, \tag{6}$$

where an effective angle θ_{ef} is a function of the similarity parameter as follows:

$$\theta_{\mathrm{ef}} = 48 + 14.12s - 22.77s^2 + 19.24s^3 \ (\mathrm{deg}), \tag{7}$$

while the $R_p(\mu_i)/R_p(1)$ ratio approximated (with the relative errors generally smaller than 10%) by the following expression:

$$\frac{R_p(\mu_i)}{R_p(1)} = \exp\{[-3.599 \ln(1-s) - 0.550 \ln^2(1-s) + 0.0416 \ln(1-g) \times \ln(1-s)](1-\mu_i)^2\} \tag{8}$$

at any values of g and $\mu_i > 0.7$. An expression for calculation of r used in the form developed by Hulst [18,31]:

$$r = \frac{(1 - 0.139s)(1-s)}{1 + 1.170s}. \tag{9}$$

The numerator of the fraction in Eq. (6) is the plane albedo at the given illumination angle normalized by the plane albedo at the vertical illumination, and the

Table 3. Accuracy of Selected Models for the Plane Albedo $R_p(\theta_i)$ at $\theta_i = 30.5°$[a]

Model	References	MAPE (%)	NRMSE (%)
$R_p(\mu_i) = \exp\left[-\frac{4(1+2\mu_i)s\sqrt{3}}{7}\right]$	[10,32]	-; 2.7; 0.7 -; 29; 0.9 -; -; 2.4	49; 3.6; 1.0 -; 24; 0.9 -; -; 6.3
$R_p(\mu_i) = \frac{0.5G}{B}\sum_{j=0}^{N}(-1)^j x_j P_j(\mu_i)Q_j(\mu_i)$, $p(\theta) = \sum_{j=0}^{N} x_j P_j(\theta)$, $Q_j(\mu_i) = \int_0^1 \frac{P_j(\mu_v)\mu_v d\mu_v}{\mu_i+\mu_v}$, where $P_j(\theta)$ are the Legendre polynomials of order j, and x_j are the expansion coefficients for a given phase function $p(\theta)$	[10,33,34]; abbreviated as GKS	5.0; 15; - 9.6; 24; - 2.4; 11; 47	12; 21; - 20; 37; - 6.3; 30; -
$R_p(\mu_i) = r\left[\frac{R_p(\mu_i)/R_p(1)}{R_p(\mu_{i,\mathrm{eff}})/R_p(1)}\right]$, $r = R_p(\mu_{i,\mathrm{eff}}) = \frac{(1-0.139s)(1-s)}{1+1.170s}$, $\frac{R_p(\mu_i)}{R_p(1)} = \exp\{[-3.599\ \ln(1-s) - 0.550 \times \ln^2(1-s) + 0.0416\ \ln(1-g) \times \ln(1-s)](1-\mu_i)^2\}$ $\mu_{i,\mathrm{eff}} = \cos\theta_{i,\mathrm{eff}}$, $\theta_{i,\mathrm{eff}} = 48 + 14.12s - 22.77s^2 + 19.24s^3$(deg)	[18,31]; current (replacement) method	44; 20; 4.4 36; 14; 1.5 27; 26; 4.1	43; 24; 3.3 36; 12; 1.3 38; 29; 0.8
$R_p(\mu_i) = (0.0001 + 0.3244G + 0.1425G^2 + 0.1308G^3)/\mu_i$	[22,35]; abbreviated as Gordon	13; 20; 26 2.7; 2.2; 15 28; 5.4; 20	22; 25; 34 3.2; 2.2; 29 7.1; 20; 33
$R_p(\mu_i) = \frac{1-\sqrt{1-\omega_0}}{1+2\mu_i\sqrt{1-\omega_0}}$	[20]; abbreviated as Hapke 1	3.5; 2.5; 1.0 -; -; 23 -; -; -	4.0; 3.0; 1.1 -; -; 13 -; -; -
$R_p(\mu_i) = \frac{1-s}{1+2\mu_i s}$	[10,18,20,31]; abbreviated as HKS 1	3.3; 2.4; 0.9 46; 20; 3.6 -; -; 19	3.9; 2.9; 1.1 48; 19; 2.1 -; -; 4.2
$R_p(\mu_i) = \Phi(\zeta_i)\frac{1-s}{1+2\mu_i s}$, $\Phi(\zeta_i) = \exp\{(A_1\zeta_i + A_2\zeta_i^2)s + (A_3\zeta_i + A_4\zeta_i^2)s^2\}$,			
$A_j = \sum_{k=1}^{3}\alpha_{jk}g^{k-1}$, $\zeta_i = \mu_i - 0.5$, $\alpha_{jk} = \begin{pmatrix} -0.991 & 3.139 & -1.874 \\ 1.435 & -4.294 & 2.089 \\ 0.719 & -5.801 & 2.117 \\ -0.509 & 0.418 & 3.360 \end{pmatrix}$	[10,18,20,31]; abbreviated as HKS 2	3.4; 0.7; 0.5 3.9; 2.0; 0.2 22; 19; 3.2	2.4; 0.9; 0.7 4.3; 1.5; 0.2 28; 19; 0.6
$R_p(\mu_i) = \frac{0.5(1-s^2)(1+2\mu_i)}{s(1+2\mu_i s)} \times \left\{1 + \frac{(1-s)\ln(1+2s)}{2s(2\mu_i s-1)} + \frac{\mu_i s(2\mu_i-1)[\ln\mu_i - \ln(1+\mu_i)]}{2\mu_i s-1}\right\}$	Derived from [18,20,31]; abbreviated as HH	4.7; 4.2; 3.4 34; 12; 1.8 -; -; 15	4.9; 4.4; 3.8 34; 10; 2.6 -; -; 4.0
$R_p(\mu_i) = 0.5\omega_0\left\{[p(\theta) - 1][1 + \mu_i\ \ln\mu_i - \ln(1+\mu_i)] + H(\mu_i)\int_0^1 \frac{H(\mu_v)\mu_v}{\mu_i+\mu_v}d\mu_v\right\}$, $H(\mu) = \{1 - \mu\omega_0[r_0 + (0.5 - \mu r_0)\ln(1+1/\mu)]\}^{-1}$, $\times \ln(1+1/\mu)]\}^{-1}$	Derived from [20,36]; abbreviated as Hapke 2	13; 9.8; 4.5 43; 33; 12 -; -; -	15; 12; 4.2 -; 28; 11 -; -; 43
$R_p(\mu_i) = \frac{(1-\bar{\mu})^2}{1+\mu_i\bar{\mu}(4-\bar{\mu}^2)}$, $\bar{\mu} = \sqrt{\frac{1+2G-\sqrt{G(4+5G)}}{1+G}}$	[4]	14; 11; 2.7 23; 26; 16 23; 28; 21	16; 13; 2.0 34; 33; 10 33; 50; 18

[a]The error values (MAPE and NRMSE) derived for the $R_p(\theta_i)$ are shown in the upper, middle, and bottom rows for the $p(\theta)$ with $g = 0.0019$, 0.5033, and 0.9583, respectively, while the error values derived for $R_p(\theta_i)$ computed for the ranges of $0.1 \le \omega_0 \le 0.6$, $0.6 \le \omega_0 \le 0.9$, and $0.9 \le \omega_0 \le 1$ are shown in the left, middle, and right columns of the same columns. Errors more than 50% are noted by "-".

denominator of the fraction is the plane albedo at the effective angle normalized by the plane albedo at the vertical illumination. Calculations carried for five very different scattering phase functions [10] show that the relative errors of Eq. (7) are generally smaller than 2%.

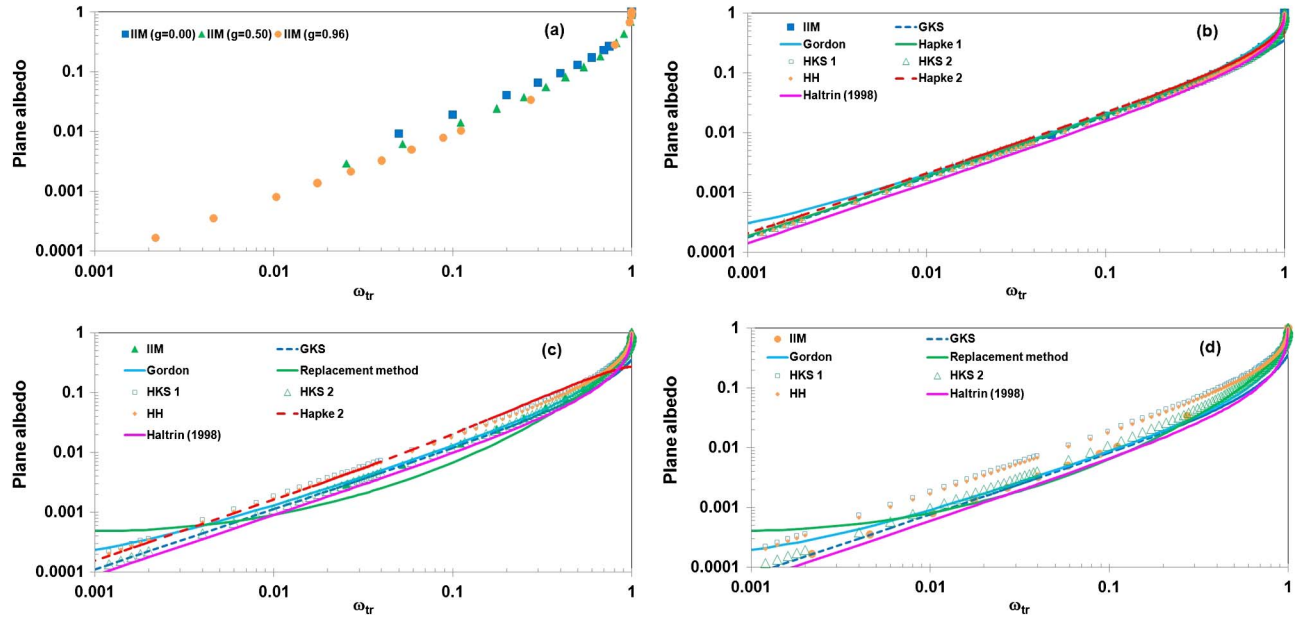

Fig. 2. Plane albedo as a function of transport single-scattering albedo ω_{tr}. (a) Computations performed by the numerical (IIM). (b)–(d) Selected analytical methods at incidence angle $\theta_i = 30.5°$ shown for three different phase functions with $g = 0.00$ [(a), (b)]; 0.50 [(a), (c)]; and 0.96 [(a), (d)].

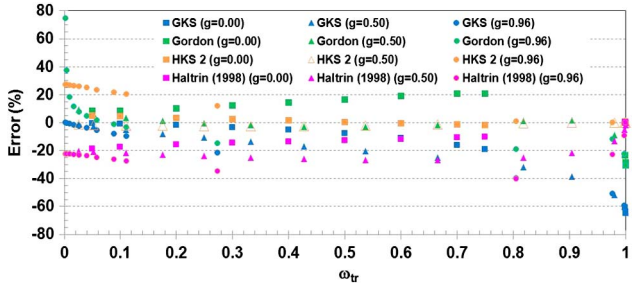

Fig. 3. Errors of selected plane albedo approximations compared to the IIM-derived values at $\theta_i = 30.5°$ for different phase functions versus ω_{tr}.

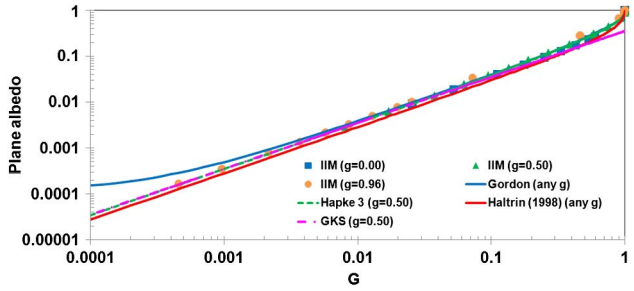

Fig. 4. Plane albedo as a function of Gordon's parameter G computed by numerical and selected analytical methods at $\theta_i = 30.5°$ for different phase functions.

2. *Hapke and van de Hulst (HH) Method*

This method was derived from the Hapke [20] expression obtained for the azimuthally averaged reflectance factor in the case of the isotropic scattering:

$$\bar{R}(\mu_i, \mu_v) = \frac{0.25\omega_0 H(\mu_i) H(\mu_v)}{\mu_i + \mu_v}, \tag{10}$$

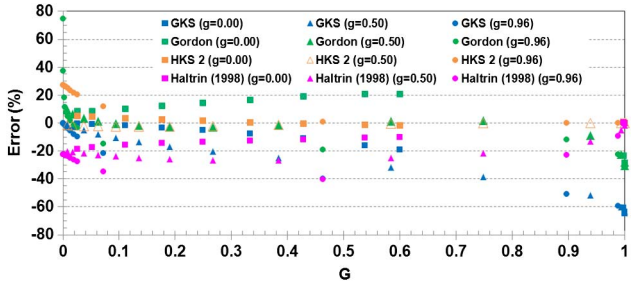

Fig. 5. Same as Fig. 3, but errors versus G.

where the Ambartsumian–Chandrasekhar function $H(\mu)$ is expressed as

$$H(\mu) = \frac{1 + 2\mu}{1 + 2\mu\sqrt{1 - \omega_0}}. \tag{11}$$

To generalize Eqs. (10) and (11) for media with arbitrary phase functions, we apply Hulst's [18,31] similarity rule using the replacement of the single-scattering albedo ω_0 by the transport (reduced) single-scattering albedo ω_{tr} and then by the similarity parameter s as follows:

$$\omega_0 = \frac{b}{a + b} \to \omega_{\mathrm{tr}} = \frac{b_{\mathrm{tr}}}{a + b_{\mathrm{tr}}} = 1 - s^2. \tag{12}$$

Then

$$\bar{R}(\mu_i, \mu_v) = \frac{0.25(1 - s^2) H(\mu_i) H(\mu_v)}{\mu_i + \mu_v} \tag{13}$$

and

$$H(\mu) = \frac{1 + 2\mu}{1 + 2\mu s}. \tag{14}$$

Finally, an expression for the $R_p(\mu_i)$ has been derived by substitution of Eqs. (13) and (14) into Eq. (2) and taking the definite integral:

$$R_p(\mu_i) = \frac{0.5(1 - s^2)(1 + 2\mu_i)}{s(1 + 2\mu_i s)} \times \left\{1 + \frac{(1 - s)\ln(1 + 2s)}{2s(2\mu_i s - 1)} + \frac{\mu_i s(2\mu_i - 1)[\ln\,\mu_i - \ln(1 + \mu_i)]}{2\mu_i s - 1}\right\}. \tag{15}$$

3. *Hapke (Hapke 2) Method*

This method uses the $\bar{R}(\mu_i, \mu_v)$ in the form derived by Hapke [20]:

$$\bar{R}(\mu_i, \mu_v) = \frac{0.25\omega_0[p(\theta) + H(\mu_i)H(\mu_v) - 1]}{\mu_i + \mu_v} \tag{16}$$

and $H(\mu)$ in the form derived by Hapke [36] for anisotropic scattering with any g:

$$H(\mu) = \{1 - \mu\omega_0[r_0 + (0.5 - \mu r_0)\ln(1 + 1/\mu)]\}^{-1},$$
$$r_0 = \frac{1 - \sqrt{1 - \omega_0}}{1 + \sqrt{1 - \omega_0}}. \tag{17}$$

Substitution of Eqs. (16) and (17) into Eq. (2) leads to expression for the $R_p(\mu_i)$:

$$R_p(\mu_i) = 0.5\omega_0\left\{[p(\theta) - 1][1 + \mu_i\,\ln\,\mu_i - \ln(1 + \mu_i)] + H(\mu_i)\int_0^1 \frac{H(\mu_v)\mu_v}{\mu_i + \mu_v}\mathrm{d}\mu_v\right\}. \tag{18}$$

An integral in Eq. (18) cannot be taken analytically; instead, we estimated it by the standard numerical method using a composite of Simpson's rule with 250 subintervals.

4. *Plane Albedo Modeling Results*

Numerical results demonstrate a great variability of different approximations for the plane albedo (Table 3 and Fig. 2), an accuracy of which mostly depends on the selected model and values of μ_i, g, and ω_0. As shown for calculations carried out by different models, the best result demonstrates the HKS 2 model at $\omega_{tr} > 0.1$; however, at smaller values of ω_{tr}, the best result was obtained by the GKS model (Fig. 3). The HKS 2 model has been first derived by Kokhanovsky and Sokoletsky [10] as a modification of Hapke [20] solution. This modification may be reduced to two subsequent steps: (1) the replacement ω_0 by the ω_{tr} according to Hulst's [18,31] similarity rule and (2) using the additional multiplicative factor $\Phi(\zeta_i)$ to improve accuracy of the model. The GKS model for the plane albedo was derived by Kokhanovsky and Sokoletsky [10] from the Gordon [33] and Golubitsky *et al.* [34] quasi-single-scattering approximation obtained initially as a solution for the reflectance factor.

Another finding is that the $R_p(\mu_i)$ is rather a function of the Gordon's parameter G (Fig. 4) than of the transport albedo ω_{tr} [Fig. 2(a)]. This fact is confirmed by the numerical and approximated computations. Especially good results were obtained by applying the Gordon, Haltrin, and GKS models. Note that in a practice if, for example, the ω_{tr} and ω_0 are known, then it is easy to find an asymmetry parameter g (see Table 1) and then to estimate a backscattering contribution B (for a given scattering phase function) and G. To show better the impact of G on $R_p(\mu_i)$, we used an alternative abscissa axis with G values (Figs. 4 and 5) for demonstrating the absolute values of $R_p(\mu_i, G)$ and relative errors for several models. Note that since the GKS and HKS 2 models give values of $R_p(\mu_i)$ almost independent on selected scattering phase functions, we have shown here the values of $R_p(\mu_i)$ obtained only for one phase function; namely, with $g = 0.50$ (Fig. 4).

Overall, among all considered approximations, the best results show the GKS approximation at $G < 0.05$ and HKS 2 approximation at all other values of G (see Fig. 5). Combined application of these two models gives a relative error $\delta < 16\%$.

5. *Plane Albedo Modeling Under Lack of $p(\theta)$ Information*

In real practice, a scattering phase function is often inaccessible. This is also means inaccessibility of information about the g, ω_{tr}, and s parameters. However, it is possible to estimate g (and, hence, ω_{tr} and s) from measured $B = b_b/b$ values. Below we suggest an algorithm for the $p(\theta)$ and g estimation and test for the impact of this inaccuracy in g on the accuracy of estimated $R_p(\mu_i)$.

For current modeling, we selected the widely applied Henyey–Greenstein $p(\theta)$:

$$p(\theta) = \frac{1 - g^2}{(1 - 2g\,\cos\,\theta + g^2)^{1.5}}. \tag{19}$$

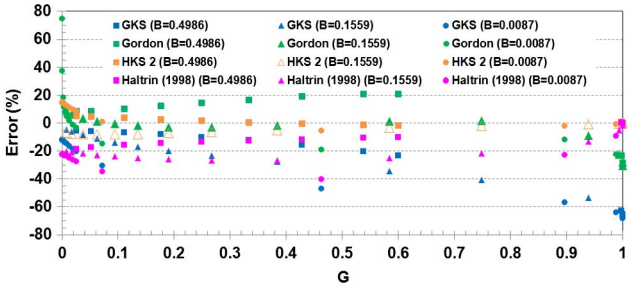

Fig. 6. Errors of selected plane albedo approximations compared to the IIM-derived values at $\theta_i = 30.5°$ for different phase functions versus G in situations when the scattering phase function is unknown.

Table 4. Accuracy of Selected Models for the Spherical Albedo r[a]

Model	References	MAPE (%)	NRMSE (%)
$r = \frac{1-\sqrt{1-G^2}}{G}$	[38–40]; abbreviated as GKM	17; 14; 1.0 18; 14; 3.7 44; 44; 18	20; 16; 1.7 22; 15; 3.5 -; -; 11
$r = \frac{\ln(1+\xi)-\xi}{\ln(1-\xi)+\xi}$, $\omega_{tr} = \frac{2\xi}{\ln[(1+\xi)/(1-\xi)]}$	[41–43]; abbreviated as CKS	17; 7.1; 0.5 15; 7.5; 0.9 -; 17; 3.8	16; 8.4; 1.0 18; 7.2; 0.9 -; 22; 1.3
$r = \exp\left(-\frac{4}{\sqrt{3}}y\right)$	[32,44]	-; 11; 0.5 -; 3.6; 0.4 -; -; 13	-; 13; 1.0 50; 3.5; 0.4 -; -; 3.6
$r = 1 + \frac{K}{S} - \sqrt{\frac{K}{S}\left(\frac{K}{S}+2\right)}$, $\frac{K}{S} = \frac{8}{3}\frac{1-\omega_{tr}}{\omega_{tr}}$	GKM; [45,46]; abbreviated as GKM + MR	7.2; 4.1; 0.5 3.4; 3.0; 0.6 0.5; 1.8; 1.1	7.5; 4.9; 1.0 4.7; 3.2; 0.6 1.0; 4.1; 0.7
$r = \frac{G}{B}\sum_{j=0}^{N}\int_0^1 (-1)^j x_j P_j(\mu_i) Q_i(\mu_i)\mu_i d\mu_i$, $p(\theta) = \sum_{j=0}^{N} x_j P_j(\theta)$, $Q_i(\mu_i) = \int_0^1 \frac{P_i(\mu_v)\mu_v d\mu_v}{\mu_i+\mu_v}$, where $P_j(\theta)$ are the Legendre polynomials of order j, and x_j are the expansion coefficients for a given phase function $p(\theta)$.	[33,34,43]; abbreviated as GSK	3.0; 12; - 1.0; 1.7; 22 0.8; 1.0; 9.1	7.9; 16; - 2.1; 1.9; 37 1.4; 1.2; 13
$r = \frac{(1-0.139s)(1-s)}{1+1.170s}$	[18,31]; abbreviated as Hulst	2.9; 1.3; 0.5 1.5; 0.2; 0.0 5.8; 3.5; 0.4	2.8; 1.5; 1.0 1.2; 0.2; 0.0 6.8; 3.2; 0.1
$r = 0.0003 + 0.3687G + 0.1802G^2 + 0.0740G^3$	[22]	4.3; 1.5; 35 36; 27; 27 47; -; 37	3.1; 2.2; 44 45; 29; 37 -; -; 43
$r = 1 + \frac{K}{S} - \sqrt{\frac{K}{S}\left(\frac{K}{S}+2\right)}$, $K = a/\eta$, $S = b_{tr}/\chi$, $\eta = \frac{1}{224}[132 - 55\omega_{tr} + 35 \times \sqrt{1 + 2(1-\omega_{tr})/35 + 121(1-\omega_{tr})^2/49}]$, $\chi = \frac{2\eta\omega_{tr}(16\eta-3)}{15\eta^2-(1-\omega_{tr})(16\eta-3)}$	GKM; [47] with the replacement: $\omega_0 \to \omega_{tr}$	10; 5.5; 0.5 27; 3.9; 0.8 -; 46; 1.4	8.7; 6.6; 1.0 13; 4.6; 0.8 -; 33; 1.0
$r = \frac{(1-0.681s)(1-s)}{1+0.792s}$	[1]	41; 24; 0.3 45; 27; 5.0 -; 48; 13	43; 29; 0.6 -; 27; 4.7 -; -; 5.7
$r = \frac{1-\exp\left(-\sqrt{24a/b_{tr}}\right)}{\sqrt{24a/b_{tr}}}\exp(-2a/b_{tr})$	[48]	-; -; 1.1 -; 19; 5.2 -; -; -	-; -; 1.8 -; 19; 5.2 -; -; 37
$r = 1 + \frac{K}{S} - \sqrt{\frac{K}{S}\left(\frac{K}{S}+2\right)}$, $K = a/\eta$, $S = b_{tr}/\chi$, $\eta = 0.25(3-\omega_{tr})$, $\chi = (98 - 38\omega_{tr})/45$	GKM; [49]; abbreviated as GS	12; 6.2; 0.5 10; 5.8; 0.8 7.9; 8.7; 2.5	12; 7.4; 1.0 11; 5.8; 0.8 11; 13; 1.1
$r = \frac{(1-\Psi)\left(\Psi-\sqrt{1+\Psi^2}\right)^2}{1+\Psi}$	[50]	11; 1.1; 0.7 44; 29; 7.0 -; -; 24	7.5; 1.4; 1.3 -; 31; 6.5 -; -; 15
$r = \frac{1-s^2}{1+\left(5\sqrt{3}/3\right)s+2s^2}$	[51]; abbreviated as Flock	17; 15; 0.2 13; 14; 5.4 9.4; 11; 7.0	21; 18; 0.3 18; 16; 5.2 14; 18; 5.7
$r = \frac{1-s}{1+s}$	Derived from [52] with the replacement: $\omega_0 \to \omega_{tr}$	17; 14; 1.0 25; 17; 4.4 33; 29; 8.4	20; 17; 1.7 29; 18; 4.1 43; 36; 4.6
$r = 0.5(1-s^2)\exp\left(-\sqrt{3}s\right) \times \left[1 + \exp\left(-\frac{4\sqrt{3}}{3}s\right)\right]$	[53]	45; 33; 0.3 46; 34; 9.4 48; 47; 17	-; 40; 0.4 -; 38; 8.8 -; -; 9.9

(Table continued)

Table 4. Continued

Model	References	MAPE (%)	NRMSE (%)
$r = (1-s)\left[\frac{1}{s} - \frac{0.5\ln(1+2s)}{s^2}\right]$	[10,20]; abbreviated as HKS 1	6.5; 4.1; 0.6 13; 6.6; 1.0 20; 16; 3.3	7.1; 5.0; 1.0 14; 6.6; 0.9 25; 19; 1.2
$r = \sqrt{6}\{2\sqrt{0.45+W} - \sqrt{W} - \sqrt{0.9+W}\}$	[54]	23; 26; 3.6 29; 32; 10 -; -; 21	34; 32; 4.4 49; 35; 9.1 -; -; 11
$r = \left(\frac{1-\bar{\mu}}{1+\bar{\mu}}\right)^2,\ \bar{\mu} = \sqrt{\frac{1+2G-\sqrt{G(4+5G)}}{1+G}}$	[4]	17; 6.7; 0.5 48; 34; 9.1 -; -; -	15; 7.9; 1.0 -; 37; 8.6 -; -; 17
$r = \frac{1+3a/b_{tr}-\sqrt{9(a/b_{tr})^2+6(a/b_{tr})}}{1+a/b_{tr}}$	[55]	-; 39; 0.3 -; 45; 7.3 -; -; 22	-; 47; 0.6 -; 45; 7.0 -; -; 8.9
$r = \exp\left[-\frac{6.374+0.3569(b_{tr}/a)^{0.2879}}{\sqrt{3(1+b_{tr}/a)}}\right]$	Derived from [56]	45; -; 3.8 -; -; 22 -; -; 26	-; -; 5.8 -; -; 21 -; -; 23
$r = \frac{\omega_{tr}}{13-12\omega_{tr}}$	[57], their Eq. (2)	-; 42; 3.4 -; 43; 10 -; -; 21	-; 50; 5.5 -; 46; 9.7 -; -; 12
$r = \frac{1}{1-13\ln\omega_{tr}}$	[57], their Eq. (10)	-; -; 1.7 -; -; 42 -; -; -	-; -; 2.7 -; -; 43 -; -; 48
$r = \exp(-2\sqrt{2.68W})$	[57], their Eq. (15)	-; -; 0.8 -; -; 14 -; -; 31	-; -; 1.2 -; -; 13 -; -; 16
$r = \frac{1}{2}\left[\exp\left(-\sqrt{3}s\right) + \exp\left(-\frac{7}{\sqrt{3}}s\right)\right]$	[57], their Eq. (16)	-; 5.2; 0.2 -; 16; 4.8 -; -; 24	-; 6.8; 0.4 -; 16; 4.8 -; -; 7.6
$r = \exp\{-\sqrt{6(1-\omega_{tr})/\omega_{tr}}\}$	Derived from [58] with the replacement: $\omega_0 \to \omega_{tr}$	-; 24; 0.3 -; 30; 3.8 -; -; 18	-; 28; 0.6 -; 29; 3.6 -; -; 5.7
$r = 1 + \frac{K}{S} - \sqrt{\frac{K}{S}\left(\frac{K}{S}+2\right)},\ \frac{K}{S} = \frac{C_0^2}{6}\frac{1-\omega_{tr}}{\omega_{tr}}$	[59]	33; 25; 0.1 37; 30; 8.8 40; 40; 16	38; 31; 0.2 47; 34; 8.3 -; -; 10
$r = 1 + \frac{K}{S} - \sqrt{\frac{K}{S}\left(\frac{K}{S}+2\right)},\ K = a/\eta,\ S = b_{tr}/\chi,$ $\eta = \frac{(\phi-1)(1-\omega_{tr})}{(\phi+1)\xi},\ \phi = \frac{\xi+\ln(1-\xi)}{\xi-\ln(1+\xi)},\ \chi = -\frac{0.5\omega_{tr}(\phi-1/\phi)}{\xi},$ $\xi = \sqrt{\frac{47}{52} + \frac{31}{49}\omega_{tr} - \frac{49}{54}\omega_{tr}^2 - \frac{17}{27}\omega_{tr}^3}$	GKM; [60]	-; 6.9; 0.7 -; 7.2; 1.5 -; -; 2.7	41; 8.2; 1.4 -; 7.0; 1.6 -; -; 1.3
$r = 1 + \frac{K}{S} - \sqrt{\frac{K}{S}\left(\frac{K}{S}+2\right)},\ K = a/\eta,$ $S = b_{tr}/\chi,$ $\eta = 1 - 0.6864\omega_{tr} - 0.1727\omega_{tr}^2 + 0.6783\omega_{tr}^3 - 0.3196\omega_{tr}^4,$ $\chi = 3.321 - 3.495\omega_{tr} + 1.777\omega_{tr}^2 - 0.2670\omega_{tr}^3$	GKM with the new equations for $\eta(\omega_{tr})$ and $\chi(\omega_{tr})$; abbreviated as GKM-new	17; 7.2; 0.5 16; 7.6; 0.8 19; 17; 3.7	16; 8.5; 0.9 18; 7.3; 0.8 25; 22; 1.3

[a]The error values (in %) derived for r computed for $p(\theta)$ with $g = 0.0019$, 0.5033, and 0.9583 are shown in the upper, middle, and bottom rows, respectively, in the columns labeled as MAPE (%) and NRMSE (%), while the error values derived for r computed for the ranges of $0.1 \le \omega_0 \le 0.6$, $0.6 \le \omega_0 \le 0.9$, and $0.9 \le \omega_0 \le 1$ are shown in the left, middle, and right columns of the same columns. Errors more than 50% are noted by "-".

The relationship between g and B is easily determined by integrating within the equation for B (see Table 1) leading to [37]

$$B = \frac{1-g}{2g}\left(\frac{1+g}{\sqrt{1+g^2}} - 1\right). \tag{20}$$

Inverting this equation and fitting it by the 5° polynomial leads to the following result:

$$g = 1 - 4.440B + 12.11B^2 - 23.87B^3 + 23.52B^4 - 9.317B^5, \tag{21}$$

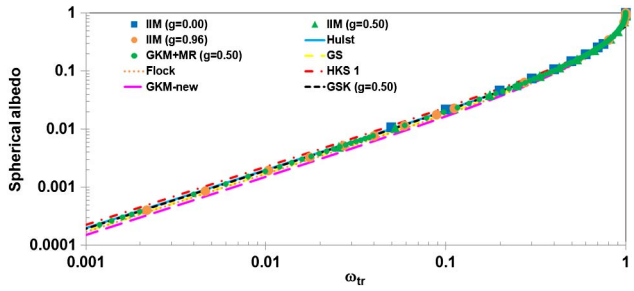

Fig. 7. Spherical albedo as a function of ω_{tr} computed by numerical and selected analytical methods for different phase functions.

with the NRMSE = 1.2% and $R^2 = 0.99998$ over the whole possible ranges of parameters B and g: $0 \le B \le 1$ and $-1 \le g \le 1$.

The values of the expansion coefficients x_j needed for computation $R_p(\mu_i)$ by the GKS model (see Table 3) may be now easily obtained from the expansion of $p(\theta)$ into the Legendre polynomial series [37]:

$$x_j = (2j+1)g^j. \tag{22}$$

The selection of Henyey–Greenstein $p(\theta)$ may be explained by its convinience for computations along with its closeness to the initial $p(\theta)$ at given values of B (see Fig. 2). The errors for the $R_p(\mu_i)$ computed for the same models that were used for plotting Fig. 6 at $\mu_i = 0.862$ and three values of B taken from the Table 2 are shown in Fig. 6 as a function of parameter G. As it follows from the computations, the inexact values of $p(\theta)$ and g lead typically to small decreases in the $R_p(\mu_i)$ values (up to 12% and 10% for GKS and HKS 2 models, respectively) comparative to the $R_p(\mu_i)$ values computed at exact (known) values of $p(\theta)$. However, an accuracy of the models under consideration is still high. The HKS 2 model is obviously better than the other models at any $p(\theta)$ and $G \ge 0.05$, while at $G < 0.05$ the best results yield a GKS model. Combined application of these two models (or only the HKS 2 model) gives a relative error $\delta < 15\%$ (Fig. 6) that is even better than an error obtained for the case of known $p(\theta)$ and g.

C. Spherical Albedo Modeling

Table 4 and Fig. 7 show various radiative transfer approximations for the spherical albedo r derived by a number of authors. The separate values of ω_0, their ranges, and scattering phase functions were selected the same as were used for the $R_p(\mu_i)$ computations. Again, all models were compared with the numerical calculations (IIM). The results show that the transport albedo ω_{tr} (or, alternatively, Hulst's similarity parameter s) better related to r than Gordon's parameter G. A logical explanation of this fact may be found on p. 211 by van de Hulst [18]. Hulst also gave numerical confirmation of this fact for the wide ranges of ω_0 (from 0.2 to 0.99) and g (from 0 to 7/8). Our work confirms this fact again.

Numerical results contained in Table 4 and shown in Figs. 7 and 8 demonstrate an excellent accuracy for Hulst's and six other testing approximations. Five of these models (Hulst, GKM + MR, Flock, HKS 1, and GSK) were considered earlier [7,9,10,43] and also demonstrated encouraging results. Two new models were analyzed now for a first time and also show reasonable results; namely, the model by Gemert and Star ("GS") and the "GKM-new" models. Both models are similar (as well as several other models listed in Table 4) and present actual attempts to express the parameters of absorption (K) and scattering (S) of the two-flux GKM theory via well-established IOPs: a, b_{tr}, and ω_{tr}.

The "GKM-new" model was developed by following [7,41,42,60] findings. More specifically, for this model

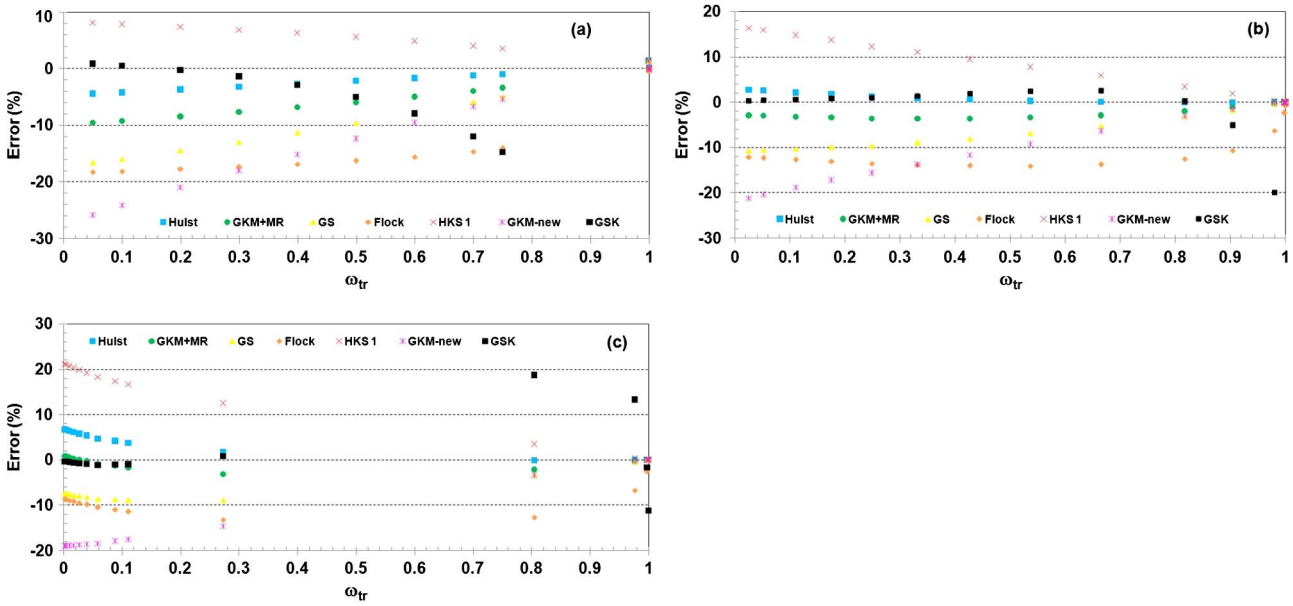

Fig. 8. Errors of selected spherical albedo approximations compared to the IIM-derived values for different phase functions versus ω_{tr}.

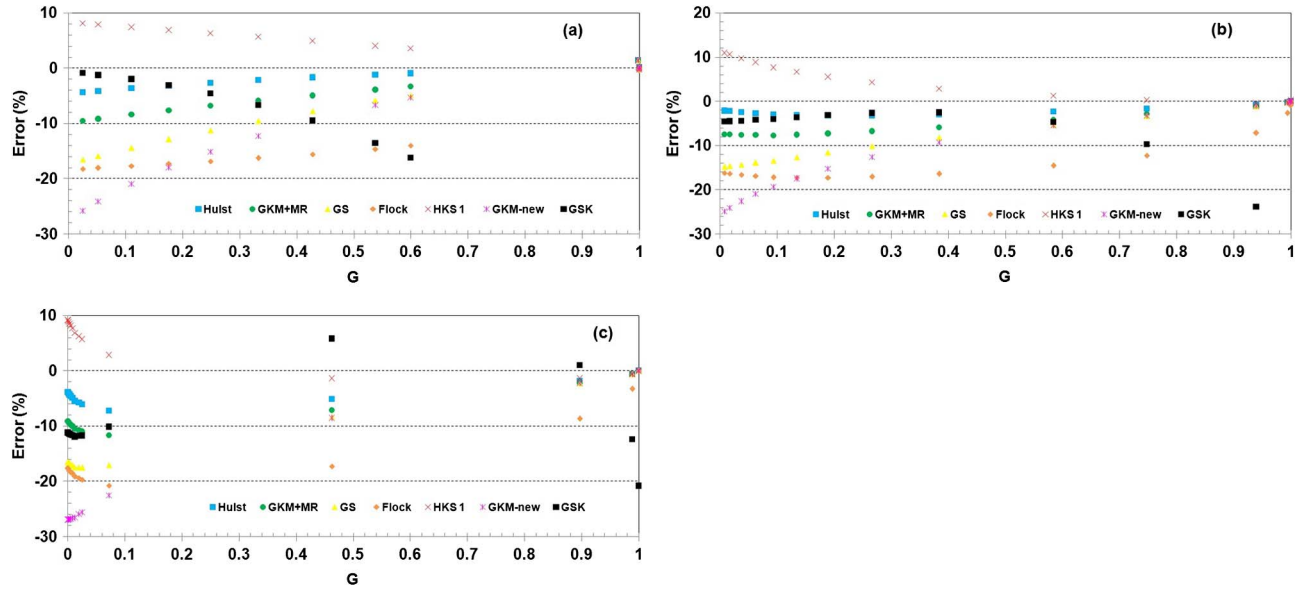

Fig. 9. Errors of selected spherical albedo approximations compared to the IIM-derived values for different phase functions versus G in situations when the scattering phase function is unknown. The values of backscattering ratio B are (a) 0.4986, (b) 0.1559, and (c) 0.0087.

we have solved a system of the equations

$$r = 1 + \frac{K}{S} - \sqrt{\frac{K}{S}\left(\frac{K}{S} + 2\right)}, \qquad r = \frac{\ln(1+\xi) - \xi}{\ln(1-\xi) + \xi},$$
$$\omega_{\mathrm{tr}} = \frac{2\xi}{\ln[(1+\xi)/(1-\xi)]}, \tag{23}$$

with the boundary conditions

$$\eta = a/K = 1 \text{ at } \omega_{\mathrm{tr}} = 0,$$
$$\eta = 0.5 \text{ at } \omega_{\mathrm{tr}} = 1, \quad \text{and}$$
$$\chi = b_{\mathrm{tr}}/S = 4/3 \text{ at } \omega_{\mathrm{tr}} = 1. \tag{24}$$

The first equation in Eq. (23) is a classical GKM, while two others were derived from the Chandrasekhar–Klier equations with Hulst's replacement: $\omega_0 \to \omega_{\mathrm{tr}}$ (CKS model) to the better accounting of a scattering anisotropy. The boundary conditions [Eq. (24)] were derived by Yudovsky and Pilon [60], and they seem as reasonable and close to conditions derived by other investigators (see Table 4). The solution has been found in the form of strictly decreasing $\eta(\omega_{\mathrm{tr}})$ and $\chi(\omega_{\mathrm{tr}})$ polynomial values that maximally satisfy Eqs. (23) and (24). A full solution presented in the Table 4 yields r values almost coinciding with the values following from the CKS model and the Yudovsky and Pilon (2009) model as well; however, their solutions failed at values $\omega_{\mathrm{tr}} < 0.06$ (or $s > 0.97$). Contrarily, the GKM-new model has a solution at any values of ω_{tr} or s. Overall, among all considered approximations, the GSK approximation demonstrated the best results at $\omega_{\mathrm{tr}} < 0.36$ (or $s > 0.80$), and the Hulst approximation is the best at the other values of ω_{tr} or s (see Fig. 8). Combined application of two these models yields a relative error $\delta < 3\%$ at any values of parameters. However, taking into account the relative complexity of the GSK model, application of only Hulst's model (with $\delta < 7\%$) also is reasonable. It is worth mentioning that the GSK approximation for the spherical albedo was derived by the direct integration (Eq. 3) from the GKS model for the plane albedo (Table 3) by Sokoletsky and Kokhanovsky [43], while Hulst's model has been developed by van de Hulst [18].

1. *Spherical Albedo Modeling Under Lack of $p(\theta)$ Information*

This is the case similar to that for the plane albedo (Subsection 3.B.5). Again, we replaced the initial $p(\theta)$ by the Henyey–Greenstein $p(\theta)$ [Eq. (19)] and the g values by their calculated values [Eq. (21)] in the cases when knowledge of $p(\theta)$ and/or g was necessary for model computations. Results show that, similarly to the $R_p(\mu_i)$ calculations, inaccurate g values lead typically to a small decrease in the r values (up to 11%) comparative to the r values computed at known (exact) values of g (Fig. 9). As before, Hulst's model demonstrates superior results in most cases with the relative errors <7%. Thus we recommend to use this spherical albedo model in the case, if the precise values of $p(\theta)$ is unknown.

D. Diffuse Reflectance Under Combined Illumination

Let us consider now a case of combined (direct and diffuse) illumination with the diffuse irradiance $I_{i,\mathrm{dif}}$ contribution d_E into the total (I_i) irradiance. Then the reflectance may be easily determined as follows:

$$R_c(\mu_i) = \frac{I_r}{I_i} = \frac{I_{i,\mathrm{dir}}(\mu_i)R_p(\mu_i) + I_{i,\mathrm{dif}}r}{I_i}$$
$$= (1 - d_E)R_p(\mu_i) + d_E r. \tag{25}$$

4. Conclusions

A large number of different approximate analytic models for plane and spherical albedo (specifically, 10 and 28 for R_p and r, respectively) of unbounded plane-parallel turbid layers were considered to reveal the most theoretically grounded and accurate models. For this aim, all models were checked for their correspondence with the physical limitations and/or compared when it was possible with the accurate numerical results. As concluded elsewhere [7] and confirmed again, among spherical albedo approximations, the Hulst and the GKM + MR models are the most accurate ones with the errors NRMSE <6.8% and 7.5%, respectively, under any optical conditions (see Table 4). The current study revealed a number of other approximations, which may also yield accurate solutions in definite situations. Such an impressive result may be explained by the fact that the r is safely governed by only one parameter, namely, s (or ω_{tr}) (Fig. 7).

A much more difficult situation is with plane albedo modeling. This property is governed by three optical parameters: μ_i, g (or B), and ω_0, though this also may be expressed by only two parameters: μ_i and ω_{tr} (Fig. 2) or μ_i and G (Fig. 4). The best result here is demonstrated in the HKS 2 and Gordon's model with the NRMSE <28% and 34%, respectively (Table 3). However, using a replacement method [Eqs. (6) to (9)] at which a calculation of the plane albedo $R_p(\mu_i)$ replaced by the calculation of the spherical albedo r also seems to be a perspective. The replacement method yields good results only at strong scattering (i.e., ω_0 close to 1) in its current form. Probably, the more complicate (and accurate) approximation for $R_p(\mu_i)/R_p(1)$ and $\theta_{i,\text{eff}}$ may help in improvement of the current solution.

The study also considers briefly the issue of the layers illuminated by combined (collimated and diffuse) light (Subsection 3.D).

The obtained results may be useful for the solution to many problems relating to the light reflected from turbid media—from very clear skies and oceanic waters to extremely turbid inland waters, biological tissues, and paint and varnishes. Better knowledge of the relationships between the measured coefficients of reflectance and the modeled IOPs (beam scattering, absorption, asymmetry parameters, etc.) will allow a more accurate solution to such problems as remote monitoring of water environments and developing multifunctional laser systems for noninvasive diagnostics.

The authors would like to acknowledge the valuable comments of Dr. Dmitrii A. Rogatkin (Moscow Regional Research and Clinical Institute "MONIKI") on earlier versions of the manuscript. The research leading to these results has received funding from the European Community's Seventh Framework Programme (FP7-PEOPLE-2009-IAPP) under grant agreement number no. 251531 (MEDI-LASE project). During the final stage of the manuscript preparation, it was also supported by the State Key Laboratory of Estuarine and Coastal Research (SKLEC) grant 2012KYYW02 and by the 111 project (B08022).

References

1. M. King and Harshvardhan, "Comparative accuracy of selected multiple scattering approximations," J. Atmos. Sci. **43**, 784–801 (1986).
2. C. D. Mobley, B. Gentili, H. R. Gordon, Z. Jin, G. W. Kattawar, A. Morel, P. Reinersman, K. Stamnes, and R. H. Stavn, "Comparison of numerical models for computing underwater light fields," Appl. Opt. **32**, 7484–7504 (1993).
3. P. E. Pierce and R. T. Marcus, "Radiative transfer theory solid color-matching calculations," Color Res. Appl. **22**, 72–87 (1997).
4. V. I. Haltrin, "Self-consistent approach to the solution of the light transfer problem for irradiances in marine waters with arbitrary turbidity, depth, and surface illumination. I. Case of absorption and elastic scattering," Appl. Opt. **37**, 3773–3784 (1998).
5. E. S. Chalhoub, H. F. Campos Velho, R. D. M. Garcia, and M. T. Vihena, "A comparison of radiances generated by selected methods of solving the radiative-transfer equation," Transp. Theory Stat. Phys. **32**, 473–503 (2003).
6. L. Sokoletsky, "A comparative analysis of selected radiative transfer approaches for aquatic environments," Appl. Opt. **44**, 136–148 (2005).
7. L. Sokoletsky, "A comparative analysis of simple radiative transfer approaches for aquatic environments," in *Proceedings of 2004 ENVISAT & ERS Symposium*, H. Lacoste, ed. (Noordwijk, 2005), pp. 1–7.
8. IOCCG Report 5, "Remote sensing of inherent optical properties: fundamentals, tests of algorithms, and applications", Z. P. Lee, ed. (Naval Research Laboratory, Stennis Space Center, 2006).
9. A. A. Kokhanovsky and L. G. Sokoletsky, "Reflection of light from semi-infinite absorbing turbid media. Part 1: spherical albedo," Color Res. Appl. **31**, 491–497 (2006).
10. A. A. Kokhanovsky and L. G. Sokoletsky, "Reflection of light from semi-infinite absorbing turbid media. Part 2: plane albedo and reflection function," Color Res. Appl. **31**, 498–509 (2006).
11. A. A. Kokhanovsky, "Physical interpretation and accuracy of the Kubelka–Munk theory," J. Phys. D **40**, 2210–2216 (2007).
12. L. G. Sokoletsky, O. V. Nikolaeva, V. P. Budak, L. P. Bass, R. S. Lunetta, V. S. Kuznetsov, and A. A. Kokhanovsky, "A comparison of numerical and analytical radiative-transfer solutions for plane albedo of natural waters," J. Quant. Spectrosc. Radiat. Transfer **110**, 1132–1146 (2009).
13. L. G. Sokoletsky, R. S. Lunetta, M. S. Wetz, and H. W. Paerl, "Assessment of the water quality components in turbid estuarine waters based on radiative transfer approximations," Isr. J. Plant Sci. **60**, 209–229 (2012).
14. J. L. Saunderson, "Calculation of the color of pigmented plastics," J. Opt. Soc. Am. **32**, 727–736 (1942).
15. A. Morel and B. Gentili, "Diffuse reflectance of oceanic waters. III. Implication of bidirectionality for the remote-sensing problem," Appl. Opt. **35**, 4850–4862 (1996).
16. C. D. Mobley, "Estimation of the remote-sensing reflectance from above-surface measurements," Appl. Opt. **38**, 7442–7455 (1999).
17. A. García-Valenzuela, F. L. S. Cuppo, and J. A. Olivares, "An assessment of Saunderson corrections to the diffuse reflectance of paint films," J. Phys. Conf. Ser. **274**, 012125 (2011).
18. H. C. van de Hulst, "The spherical albedo of a planet covered with a homogeneous cloud layer," Astron. Astrophys. **35**, 209–214 (1974).
19. T. Nakajima and M. D. King, "Asymptotic theory for optically thick layers: application to the discrete ordinates method," Appl. Opt. **31**, 7669–7683 (1992).
20. B. Hapke, *Theory of Reflectance and Emittance Spectroscopy* (University Press, 1993).

21. F. E. Nicodemus, J. C. Richmond, J. J. Hsia, I. W. Ginsberg, and T. Limperis, "Geometrical considerations and nomenclature for reflectance" (National Bureau of Standards, U.S. Department of Commerce, 1977).
22. H. R. Gordon, O. B. Brown, and M. M. Jacobs, "Computed relationships between the inherent and apparent optical properties of a flat homogeneous ocean," Appl. Opt. **14**, 417–427 (1975).
23. V. V. Sobolev, *Light Scattering in Planetary Atmospheres* (Pergamon, 1975).
24. A. A. Kokhanovsky, *Light Scattering Media Optics* (Springer-Praxis, 2004).
25. J. M. Dlugach and E. G. Yanovitskij, "The optical properties of Venus and the Jovian planets. II. Methods and results of calculations of the intensity of radiation diffusely reflected from semi-infinite homogeneous atmospheres," Icarus **22**, 66–81 (1974).
26. L. C. Henyey and J. L. Greenstein, "Diffuse radiation in the galaxy," Astrophys. J. **93**, 70–83 (1941).
27. H. M. Nussenzveig, "The theory of the rainbow," Sci. Am. **236**, 116–127 (1977).
28. H. C. van de Hulst, *Light Scattering by Small Particles* (Dover, 1981).
29. A. A. Kokhanovsky, "The determination of the effective radius of drops in water clouds from polarization measurements," Phys. Chem. Earth B **25**, 471–474 (2000).
30. M. I. Mishchenko, J. M. Dlugach, E. G. Yanovitskij, and N. T. Zakharova, "Bidirectional reflectance of flat, optically thick particulate layers: an efficient radiative transfer solution and applications to snow and soil surfaces," J. Quant. Spectrosc. Radiat. Transfer **63**, 409–432 (1999).
31. H. C. van de Hulst, *Multiple Light Scattering* (Academic, 1980), Vol. **2**.
32. O. V. Bushmakova, E. P. Zege, and I. L. Katsev, "On asymptotic equations for brightness coefficients of optically thick light scattering layers," Doklady Acad. Sci. BSSR **15**, 309–311 (1971).
33. H. G. Gordon, "Simple calculation of the diffuse reflectance of ocean," Appl. Opt. **12**, 2803–2804 (1973).
34. B. M. Golubitsky, I. M. Levin, and M. V. Tantashev, "Brightness coefficient of a semi-infinite layer of sea water," Izv. Atmos. Ocean. Phys. **10**, 1235–1238 (1974).
35. H. G. Gordon, "Dependence of the diffuse reflectance of natural waters on the sun angle," Limnol. Oceanogr. **34**, 1484–1489 (1989).
36. B. Hapke, "Bidirectional reflectance spectroscopy. 5. The coherent backscatter opposition effect and anisotropic scattering," Icarus **157**, 523–534 (2002).
37. V. I. Haltrin, "One-parameter two-term Henyey–Greenstein phase function for light scattering in seawater," Appl. Opt. **41**, 1022–1028 (2002).
38. M. Gurevich, "Über eine rationelle klassifikation der lichtenstreuenden medien," Physikalische Zeitschrift **31**, 753–763 (1930).
39. P. Kubelka and F. Munk, "Ein beitrag zur optik der farbanstriche," Zeitschrift für Technische Physik. **12**, 593–601 (1931).
40. P. Kubelka, "New contributions to the optics of intensely light-scattering material. Part I," J. Opt. Soc. Am. **38**, 448–457 (1948).
41. S. Chandrasekhar, *Radiative Transfer* (Dover, 1960).
42. K. Klier, "Absorption and scattering in plane parallel turbid media," J. Opt. Soc. Am. **62**, 882–885 (1972).
43. L. G. Sokoletsky and A. A. Kokhanovsky, "Reflective characteristics of natural waters: The accuracy of selected approximations," in *Proceedings of the D. S. Rozhdestvensky Third International Conference: Current Problems in Optics of Natural Waters*, I. Levin and G. Gilbert, eds. (Saint-Petersburg, Russia, 2005), pp. 56–63.
44. G. V. Rozenberg, "Light characteristics of thick layers of a weakly absorbing scattering medium," Doklady Acad. Sci. USSR **145**, 775–777 (1962).
45. L. W. Richards, "The calculation of the optical performance of paint films," J. Paint Technol. **42**, 276–286 (1970).
46. P. S. Mudgett and L. W. Richards, "Multiple scattering calculations for technology," Appl. Opt. **10**, 1485–1502 (1971).
47. W. E. Meador and W. R. Weaver, "Diffusion approximation for large absorption in radiative transfer," Appl. Opt. **18**, 1204–1208 (1979).
48. R. F. Bonner, R. Nossal, S. Havlin, and G. H. Weiss, "Model for photon migration in turbid biological media," J. Opt. Soc. Am. A **4**, 423–432 (1987).
49. M. J. C. Gemert and W. M. Star, "Relations between the Kubelka–Munk and the transport equation models for anisotropic scattering," Lasers Life Sci. **1**, 287–298 (1987).
50. V. I. Haltrin, "Exact solution of the characteristic equation for transfer in the anisotropically scattering and absorbing medium," Appl. Opt. **27**, 599–602 (1988).
51. S. T. Flock, M. S. Patterson, B. C. Wilson, and D. R. Wyman, "Monte Carlo modeling of light propagation in highly scattering tissues I: model predictions and comparison with diffusion theory," IEEE Trans. Biomed. Eng. **36**, 1162–1168 (1989).
52. J. F. Cornet, C. G. Dussap, and G. Dubertret, "A structured model for simulation of cultures of the cyanobacterium *Spirulina platensis* in photobioreactors I: coupling between light transfer and growth kinetics," Biotechnol. Bioeng. **40**, 817–825 (1992).
53. T. J. Farrell, M. S. Patterson, and B. Wilson, "A diffusion theory model of spatially resolved, steady state diffuse reflectance for the noninvasive determination of tissue optical properties *in vivo*," Med. Phys. **19**, 879–888 (1992).
54. J. Wu, F. Partovi, M. S. Field, and R. P. Rava, "Diffuse reflectance from turbid media: an analytical model of photon migration," Appl. Opt. **32**, 1115–1121 (1993).
55. G. H. Weiss, J. M. Porrà, and J. Masoliver, "The continuous-time random walk description of photon motion in an isotropic medium," Opt. Commun. **146**, 268–276 (1998).
56. S. L. Jacques, "Diffuse reflectance from a semi-infinite medium," 1999, http://omlc.ogi.edu/news/may99/rd/index.html.
57. G. Zonios and A. Dimou, "Modeling diffuse reflectance from semi-infinite turbid media: application to the study of skin optical properties," Opt. Express **14**, 8661–8674 (2006).
58. G. L. Rogers, "Multiple path analysis of reflectance from turbid media," J. Opt. Soc. Am. A **25**, 2879–2883 (2008).
59. S. N. Thennadil, "Relationship between the Kubelka–Munk scattering and radiative transfer coefficients," J. Opt. Soc. Am. A **25**, 1480–1485 (2008).
60. D. Yudovsky and L. Pilon, "Simple and accurate expressions for diffuse reflectance of semi-infinite and two-layer absorbing and scattering media," Appl. Opt. **48**, 6670–6683 (2009).